Optimizing Berthing of Crew Transfer Vessels against Floating Wind Turbines: A Comparative Study of Various Floater Geometries

Laurent Barthélemy

Chapter

Optimizing Berthing of Crew Transfer Vessels against Floating Wind Turbines: A Comparative Study of Various Floater Geometries

Laurent Barthélemy

Abstract

Securing the return on investment for commercial floating wind farms by a proper estimate of the operation and maintenance (O and M) downtime is a key issue to triggering final investment decisions. That is why crew transfer vessel (CTV) weather stand-by issues should be assessed together with new floating wind floater concepts, to boost their cost attractivity. However, such issues as the numerical investigation of the landing manoeuvre of a service ship against a floater reveal complex to calculate. Based on similarities with seakeeping, we investigate various floater geometries. To estimate the weather limitations associated with each configuration. Most recent works find that calculation compares with 5% accuracy to an experiment from a test tank at a model scale. Method description: (A) Vessel seakeeping: (1) assess vessel responses (amplitude and phase angles) and (2) compare them with vessel responses of available publications, as a benchmark. (B) Vessel berthing: (1) model both vessel and floater, (2) account for the wave masking effect of existing floater designs, and (3) compare the ratio of wave vertical force over wave horizontal force and the grip coefficient at the interface between the vessel fender and the floater boat landing. Findings: The wave masking effect calculation for a square floater is cross-checked favorably with an existing demonstrator.

Keywords: operation and maintenance, crew transfer vessel, floating wind farm, significant wave height, wave period

1. Introduction

The development of floating wind farms implies the issue of offshore O and M workers safety. It is therefore of upmost importance to know the constraints and acceptable conditions for berthing a CTV.

For berthing with the "bump and jump" method, a CTV comes and pushes its fender against the boat landing ladder. The fender studied here is the stiff fender [1].

The present work relies on the results of a study performed by HSVA [2] and endeavors to meet the results obtained in its CTV model tank test. However, our approach here is different from HSVA numerical berthing calculations, which are more sophisticated.

2. Method description

2.1 General

The calculation is based on a simplified linear diffraction-radiation model applied in the frequential domain [1].

The studied ship is a CATamaran CTV (CAT CTV) [2, 3]: 27 m long, 8.2 m wide, twin hulls 3.2 m wide. It is modelled with Wigley hulls (**Figure 1**) [1].

The software used are GMSH for meshing [4] and NEMOH for hydrodynamics [5].

2.2 Loads of a unidirectional wave on CTV (seakeeping)

The Wigley hull, due to the wave excitation, moves in a vertical plane as follows (**Figure 2**) [1]:

1 rotation against her floatation centre	1 degree of freedom	θ (pitch)
1 translation against her original position O	2 degrees of freedom	τx (surge) τz (heave)

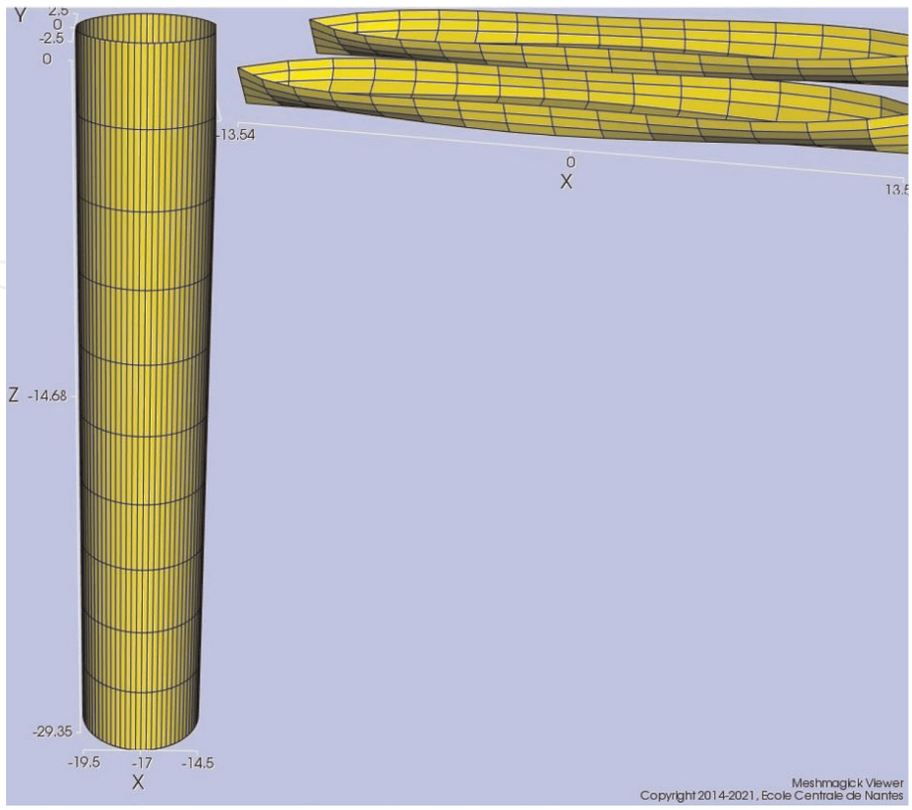

Figure 1.
CTV berthing against monopile (3D view).

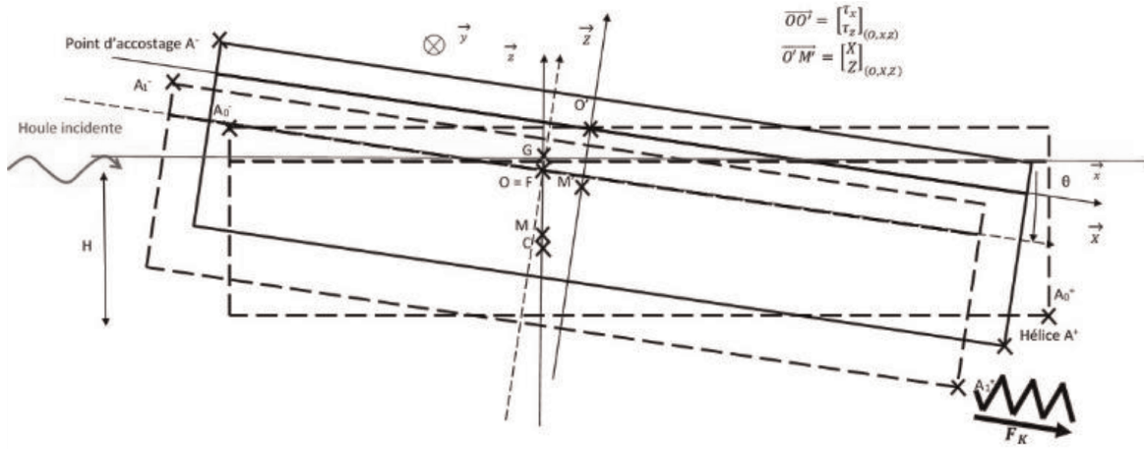

Figure 2.
CTV sea keeping without berthing (elevation).

The equations of dynamics are:

$$\begin{aligned}&(I + I_a)\ddot{X} + B\dot{X} + KX = F_{excit}\\ &\Rightarrow I\ddot{X} = F_{excit} - I_a\ddot{X} - B\dot{X} - KX \Rightarrow I\ddot{X} = \sum F_{ext}\end{aligned} \quad (1)$$

$I = \begin{bmatrix} I_{11} & 0 & I_{15} \\ 0 & I_{33} & 0 \\ I_{15} & 0 & I_{55} \end{bmatrix} = \begin{bmatrix} m & 0 & mZ_G \\ 0 & m & 0 \\ mZ_G & 0 & I_G + mZ_G^2 \end{bmatrix}$	F_{excit}: vector of wave loads I_a: matrix of added inertia (both calculated by NEMOH [5])
$B = B_R + B_V, B_V = \begin{bmatrix} \Lambda H & 0 & -\Lambda\frac{H^2}{2} \\ 0 & b_3 & 0 \\ -\Lambda\frac{H^2}{2} & 0 & \Lambda\frac{H^3}{3} \end{bmatrix}$	$b_3 \stackrel{def}{=} 2\rho BC\sqrt{gH} \times b_c$ $\lambda \stackrel{def}{=} \Lambda\omega$ with : $\Lambda \stackrel{def}{=} 4\rho CC_d(x_{max} + H\theta_{max})/(3\pi)$ B_R = radiation damping matrix (calculated with NEMOH [5]) B_V = linearised viscous damping matrix
$K = \begin{bmatrix} 0 & 0 & 0 \\ 0 & PBCG & +P \\ 0 & -P & -mgCG + mg\frac{B^2}{12H} \end{bmatrix}$	P = propeller thrust. If: $P = (m + m_a)a\sqrt{g/h}\omega$ then $\lim_{k\to 0} x_m/a = 0$

2.3 Loads of a unidirectional wave on CTV (berthing)

The friction coefficient without sliding is, about the principle of action and reaction (**Figure 3**) [1]:

$$f = \frac{\text{Tangential force at vertical wall}}{\text{Normal force at vertical wall}} = \frac{T}{N} \Longrightarrow f = \left(-\sum F_{ext\ z}\right)/\left(-\sum F_{ext\ x}\right) \quad (2)$$

Assumptions:

1. A thrust P is added to N, in order never to reach $N < 0$:

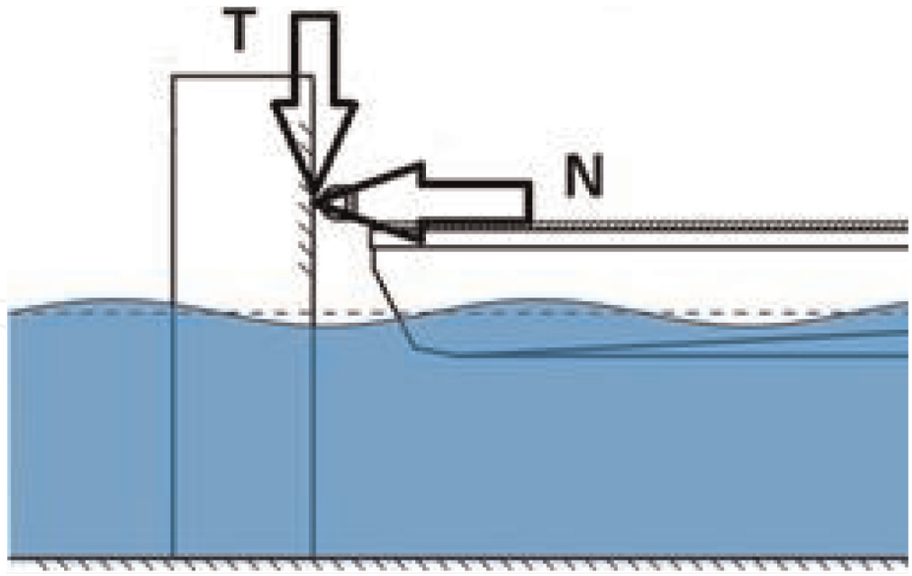

Figure 3.
Coulomb's friction law.

$$\vec{P} = -\left\|\vec{P}\right\|\vec{x} = m\omega^2 \mathcal{G}\vec{x} (\text{avec } P < 0 \text{ et } \mathcal{G} < 0) \tag{3}$$

2. For a low friction berthing:

$$\Sigma F_{ext\ z} = I_{33}\ddot{Z} \tag{4}$$

The equations at the berthing point A = A- become therefore:

$$\sum F_{ext\ z} = I_{33}\ddot{Z} \text{ and } \sum F_{ext\ x} + P = I_{11}\ddot{X} + I_{15}\ddot{\theta} \tag{5}$$

$$\Rightarrow f = \frac{-I_{33}\ddot{Z}}{-I_{11}\ddot{X} - I_{15}\ddot{\theta} + P} \Longrightarrow f = \frac{-\ddot{Z}}{-\ddot{X} - Z_G\ddot{\theta} + \mathcal{G}\omega^2} \text{where } \mathcal{G} = P/\left[m\left(1 + C'_{M1}\right)\omega^2\right] \tag{6}$$

We define t_T and t_N respectively as the time phase corrections required to get the calculated loads T(t) and N(t) in phase with HSVA test results T_{HSVA} (t) and N_{HSVA} (t) [2].

$$\begin{aligned} Z &= Z_m \text{COS}[\omega(t - t_T) + \varphi_z] \\ X &= X_m \text{COS}[\omega(t - t_N) + \varphi_x] \\ \theta &= \theta_m \text{COS}[\omega(t - t_N) + \varphi_\theta] \end{aligned} \tag{7}$$

We also define the following notations:

$$\begin{aligned} &T \stackrel{\text{def}}{=} \tan(\omega t/2) \\ &A \stackrel{\text{def}}{=} Z_m \cos(-\omega t_T + \varphi_z), \\ &B \stackrel{\text{def}}{=} Z_m \sin(-\omega t_T + \varphi_z), \\ &C \stackrel{\text{def}}{=} X_m \cos(-\omega t_N + \varphi_x) + Z_G\theta_m \cos(-\omega t_N + \varphi_\theta), \\ &D \stackrel{\text{def}}{=} X_m \sin(-\omega t_N + \varphi_x) + Z_G\theta_m \sin(-\omega t_N + \varphi_\theta) \\ &\Rightarrow f = \left[-AT^2 - 2BT + A\right]/\left[-(C - \mathcal{G})T^2 - 2DT + (C + \mathcal{G})\right] \end{aligned} \tag{8}$$

In order for the function f(t) to get relative extremes, the numerator of the quotient in Eq. (8) must have a positive discriminant δ′:

$$\delta' > 0 \Leftrightarrow |P| > m\omega^2 \sqrt{(AD - BC)^2)} / \sqrt{A^2 + B^2} \tag{9}$$

Moreover, the denominator in Eq. (8) must never be null. Physically that means that the CTV propeller thrust P should be great enough in order never to get $N < 0$. Mathematically that implies both that its discriminant Δ' must be negative and that $(\mathcal{G} - C) < 0$:

$$\Delta' < 0 \text{ and } (\mathcal{G} - C) < 0 \Leftrightarrow |P| > m\omega^2 \sqrt{D^2 + C^2} \tag{10}$$

If the conditions (3) and (4) are met, then, over a wave period, the friction coefficient will reach its extremes at the instants t_+ and t_-, which correspond to the following values T_+ and T_-:

$$T_\pm = \left[A\mathcal{G} \pm \sqrt{\left(A^2 + B^2\right)\mathcal{G}^2 - (AD - BC)^2} \right] / [AD - BC + B\mathcal{G}] \tag{11}$$

Then the maximum friction coefficient over a wave period is:

$$|f_{max}(T)| = \max [|f(T_+)|, |f(T_-)|] \tag{12}$$

We must therefore choose. Physically, that is the CTV surge over which the CTV captain has the time to adjust the propeller thrust P, in order for the fender never to lose contact with the boat landing. Nevertheless, the CTV is limited by her maximum thrust P_{max}. We infer that:

$$|P| = \min \left(m|\mathcal{G}|\omega^2, |P_{max}|\right) \tag{13}$$

Or, in other words:

$$\mathcal{G} = -\min \left(L, |P_{max}| / \left[m\omega^2\right]\right) \tag{14}$$

The selected criterion for CTV boarding at the berthing point is that the friction coefficient must never exceed the grip factor:

$$|f_{max}(T)| < f_{grip} \text{ with } f_{grip} = 0,8 \left(\text{rubber} - \text{very wet soil [6]}\right) \tag{15}$$

3. CTV against monopile

For benchmarking purpose, the first calculation models the "bump and jump" against a monopile (**Figures 1** and **4**). The water depth is 29 m.

The studied monopile has a 5 m diameter [2].

It may be noted that the CAT CTV is wider than the monopile: therefore the former is not masked from the waves by the latter.

Figure 5 compares for 2 m significant wave height (Hs) the calculated ratio of wave vertical force over wave horizontal force (T/N) with the grip coefficient of rubber against very wet soil (f_{grip}) [6].

For comparison reference [7] estimates the berthing limit to be for a ratio wavelength over boat length of 1.85 (λ/B): both results meet with 5% accuracy.

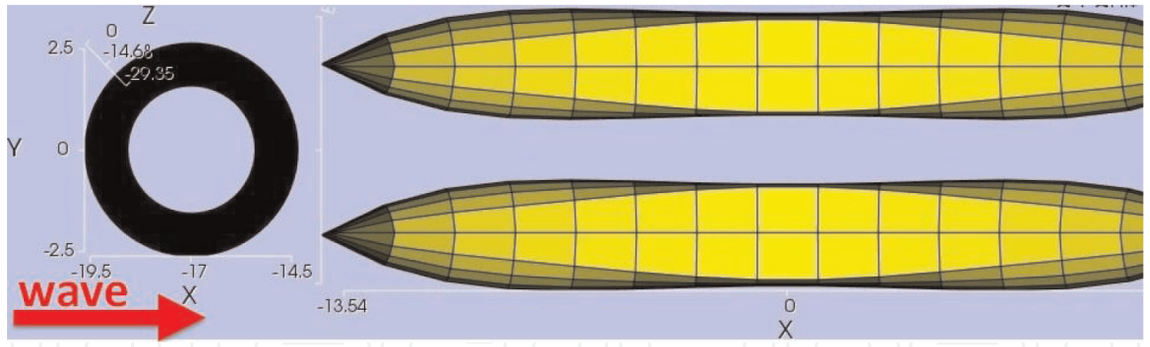

Figure 4.
CTV berthing against monopile (plane view).

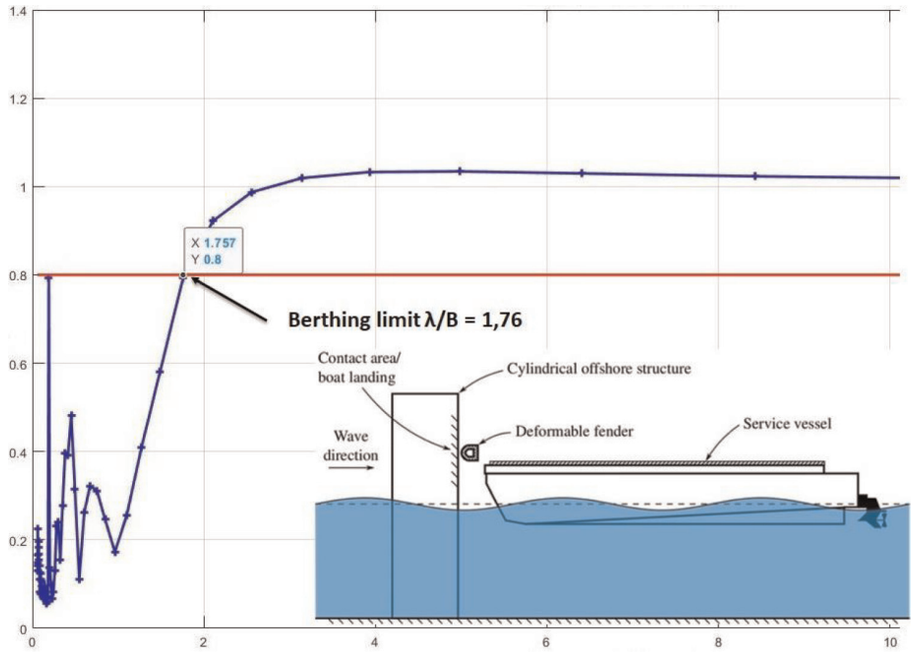

Figure 5.
Curves T/N and f_{grip} versus wavelength over boat length for 2 m Hs.

4. CTV against 13 m diameter cylindrical floater

The second calculation models the "bump and jump" against a planned [8] cylindrical wind turbine floater (**Figures 6** and 7). The water depth is 70 m [8].

The studied cylinder has [8]: a 13 m diameter, 14 m draft, 2000 T displacement.

This time, the floater masks the CAT CTV from the incidental waves, therefore the horizontal incident wave loads are masked, while the vertical incident wave loads are only the ones passing below the floater keel.

Figure 8 compares for 2 m Hs the calculated ratio T/N with f_{grip} versus λ/B.

This time berthing may take place for 2 m Hs whatever the wavelength.

5. CTV against 41 m diameter cylindrical floater

The third calculation models the "bump and jump" against a cylindrical wind turbine floater (**Figures 9** and **10**). The water depth is 23 m.

The studied cylinder has: a 41 m diameter, 7 m draft, 9300 T displacement.

DOI: http://dx.doi.org/10.5772/intechopen.102012

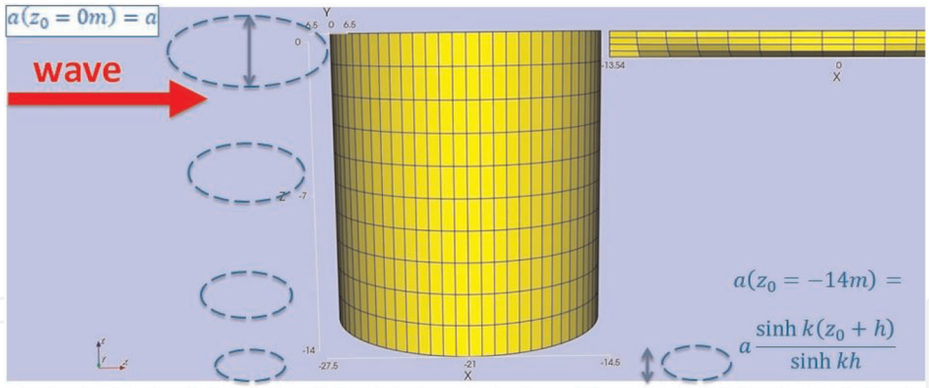

Figure 6.
CTV berthing against 13 m diameter cylindrical floater (3D view).

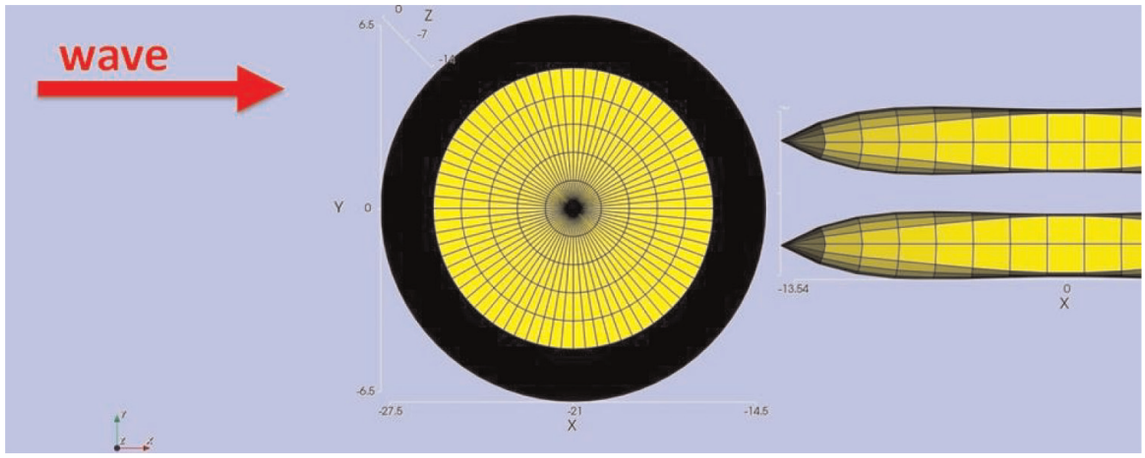

Figure 7.
CTV berthing against 13 m diameter cylindrical floater (plane view).

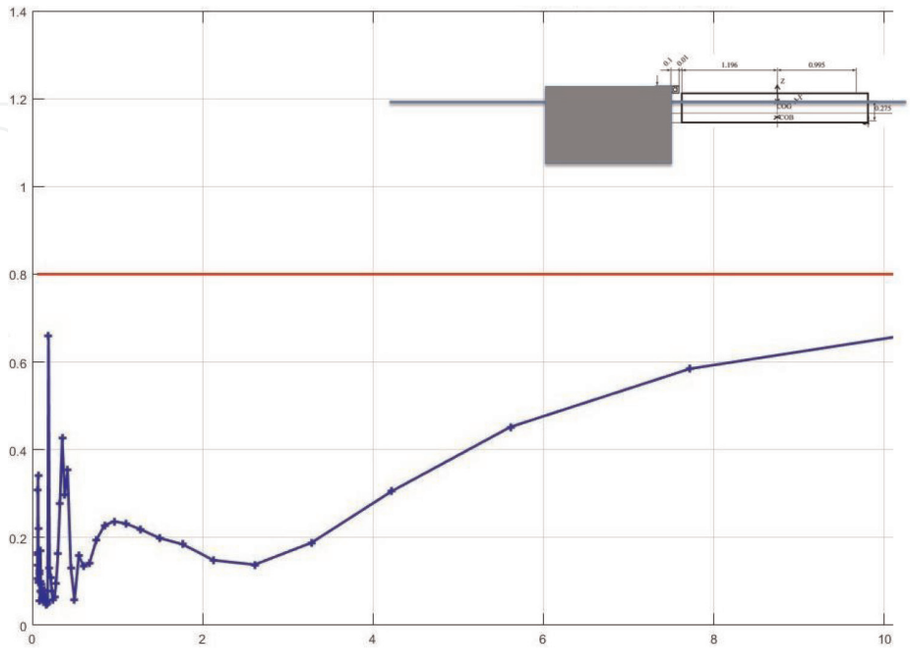

Figure 8.
Curves T/N and f_{grip} versus λ/B for 2 m Hs.

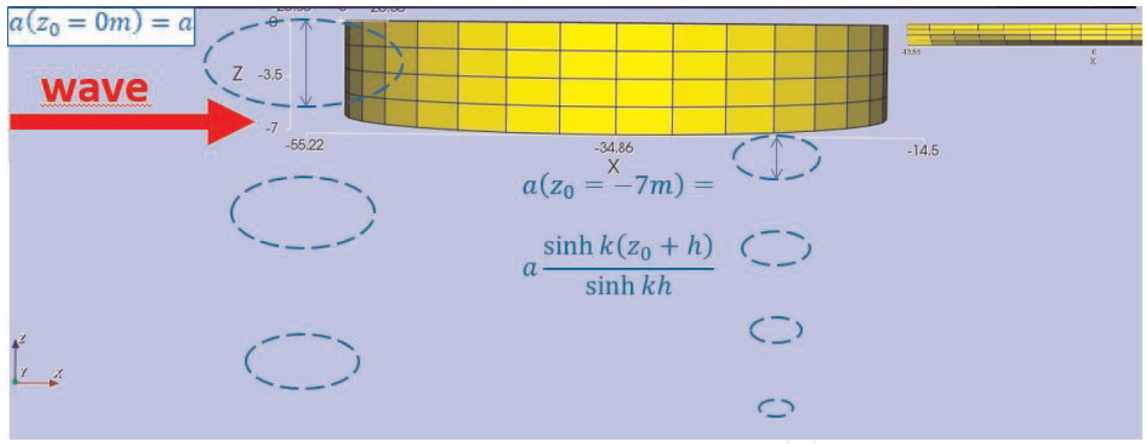

Figure 9.
CTV berthing against 41 m diameter cylindrical floater (3D view).

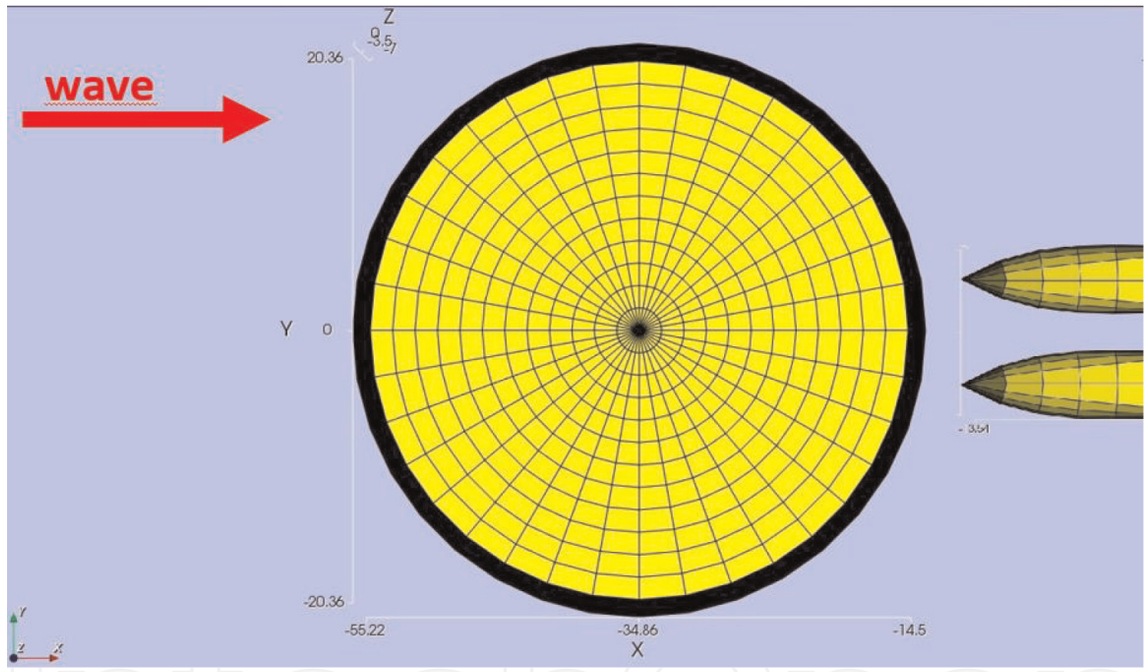

Figure 10.
CTV berthing against 13 m diameter cylindrical floater (plane view).

One more time, the floater masks the CAT CTV from the incidental waves, therefore the horizontal incident wave loads are masked, while the vertical incident wave loads are only the ones passing below the floater keel.

Figure 11 compares for 2 m Hs the calculated ratio T/N with f_{grip} versus λ/B.

This time berthing may take place for 2 m Hs whatever the wavelength.

6. CTV against 36 m side parallelepipedal floater

The fourth calculation models the "bump and jump" against a parallelepipedal wind turbine floater (**Figures 12** and **13**). The water depth is 23 m.

The studied cylinder has: a 36 m sides, 7 m draft, 9300 T displacement (same draft and displacement as in Section 5).

DOI: http://dx.doi.org/10.5772/intechopen.102012

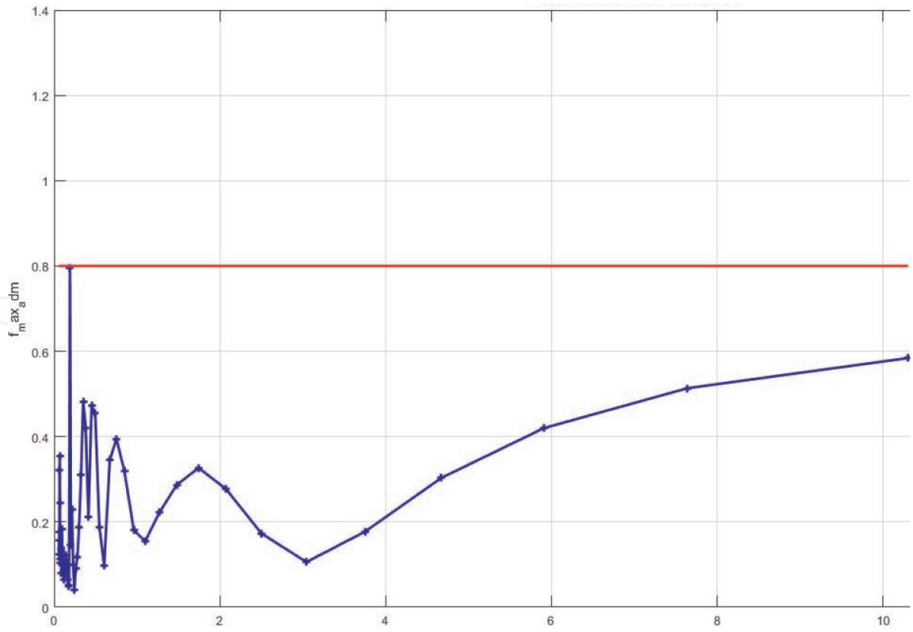

Figure 11.
Curves T/N and f_{grip} versus λ/B for 2 m Hs.

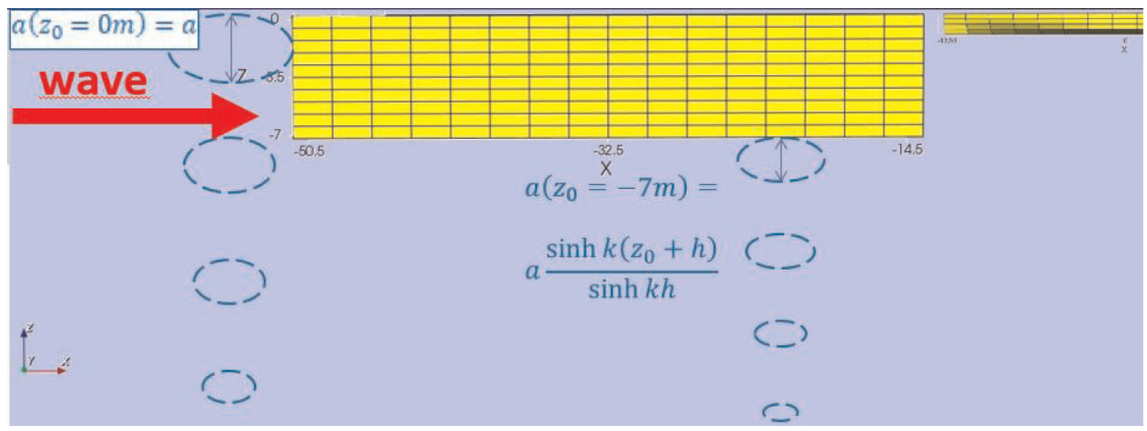

Figure 12.
CTV berthing against 36 m side parallelepipedal floater (3D view).

One more time, the floater masks the CAT CTV from the incidental waves, therefore the horizontal incident wave loads are masked, while the vertical incident wave loads are only the ones passing below the floater keel.

Figure 14 compares for 2 m Hs the calculated ratio T/N with f_{grip} versus λ/B.

This time berthing may take place for 2 m Hs whatever the wavelength.

7. CTV against FLOATGEN floater

The fifth calculation models the "bump and jump" against an existing [9] square hollow floater (**Figures 15** and **16**). The water depth is 23 m [10].

The studied square has [9, 10]: 36 m side, 7 m draft, 6000 T displacement (same draft as in Sections 5 and 6).

Once again, the floater masks the CAT CTV from the incidental waves, therefore the horizontal incident wave loads are masked, while the vertical incident wave loads are only the ones passing below the floater keel.

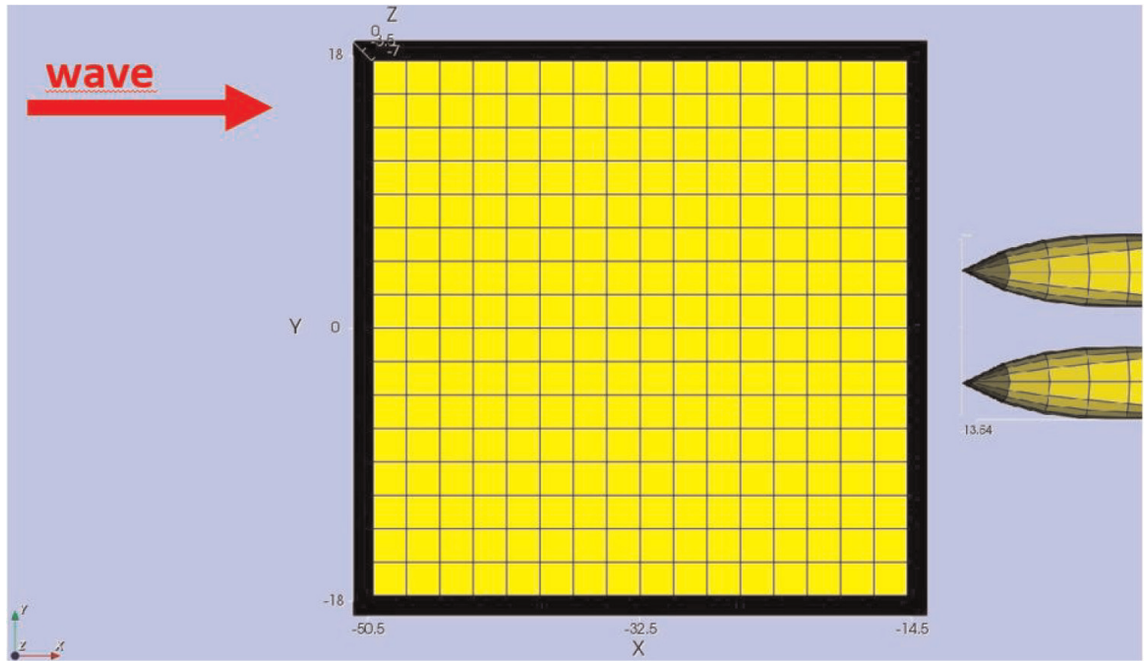

Figure 13.
CTV berthing against 36 m side parallelepipedal floater (plane view).

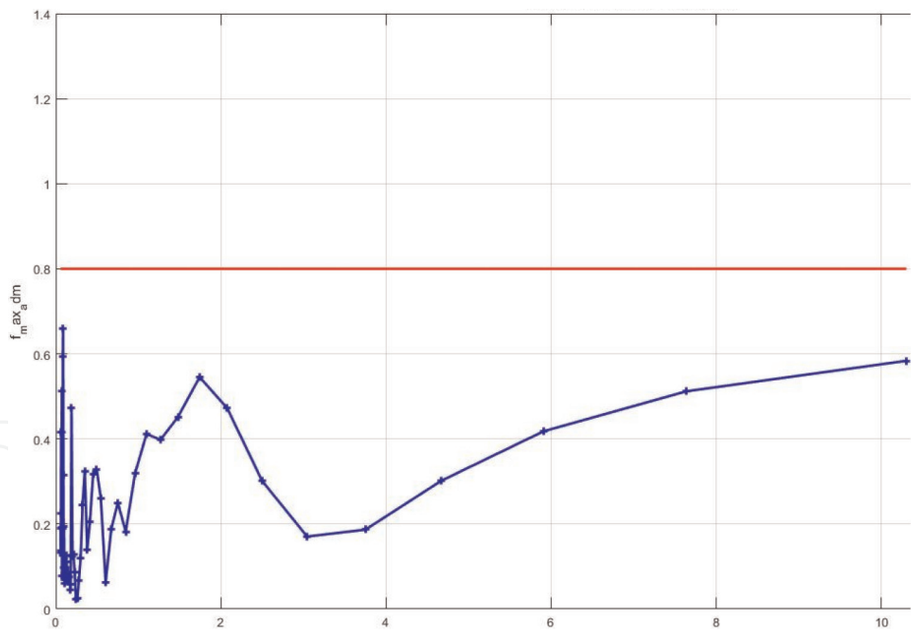

Figure 14.
Curves T/N and f_{grip} versus λ/B for 2 m Hs.

Figure 17 compares for 2 m Hs the calculated ratio T/N with f_{grip} versus λ/B. One more time berthing may take place for 2 m Hs whatever the wavelength.

8. Results

Table 1 sums up the Hs found for berthing to occur whatever the wavelength.

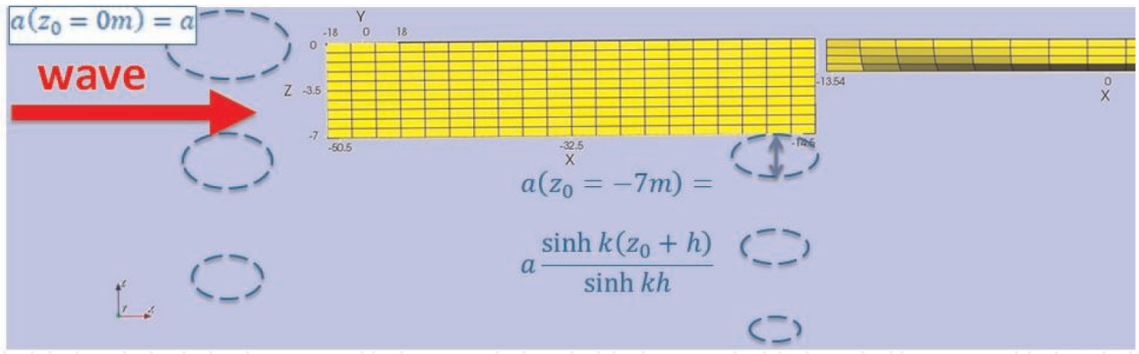

Figure 15.
CTV berthing against FLOATGEN floater (elevation).

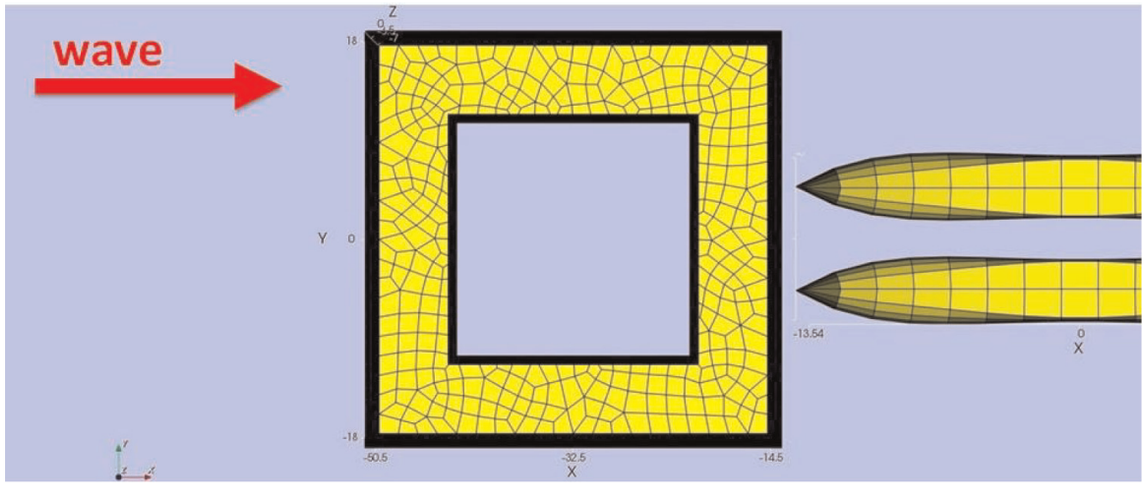

Figure 16.
CTV berthing against FLOATGEN floater (plane view).

9. Interpretations

9.1 General

FLOATGEN 2.3 m Hs berthing limit calculations compare precisely with feedback from offshore site test with full scale prototype [11]:

"Transfer up to 2.3 m significant wave height with no motion compensation".

From **Table 1**, it may be noted that berthing limits are influenced by:

- Hardly by floater geometry if they have the same displacement.
- Significantly by their displacement: the greater the displacement, the greater the berthing limit.

It is possible to propose an approximative analytical of the berthing limit due to the floater masking effect. Indeed, the calculated ratio T/N is (see Eq. (8)):

$$f(T_{\pm}) = \frac{AT_{\pm}^2 + 2BT_{\pm} - A}{(C - \mathcal{G})T_{\pm}^2 + 2DT_{\pm} - (C + \mathcal{G})} \tag{16}$$

Case	Floater geometry	Depth	Maximum Hs for berthing
1	5 m diameter monopile	23 m	1.5 m (no masking)
2	13 m diameter cylindrical floater	70 m	2.1 m
3	41 m diameter cylindrical floater[1]	23 m	2.5 m
4	36 m side square floater[1]	23 m	2.6 m
5	36 m side square hollow floater (FLOATGEN)	23 m	2.3 m

[1]*Those floaters have been chosen to have same displacement and draft.*

Table 1.
CAT CTV berthing limits for monopile various floater designs.

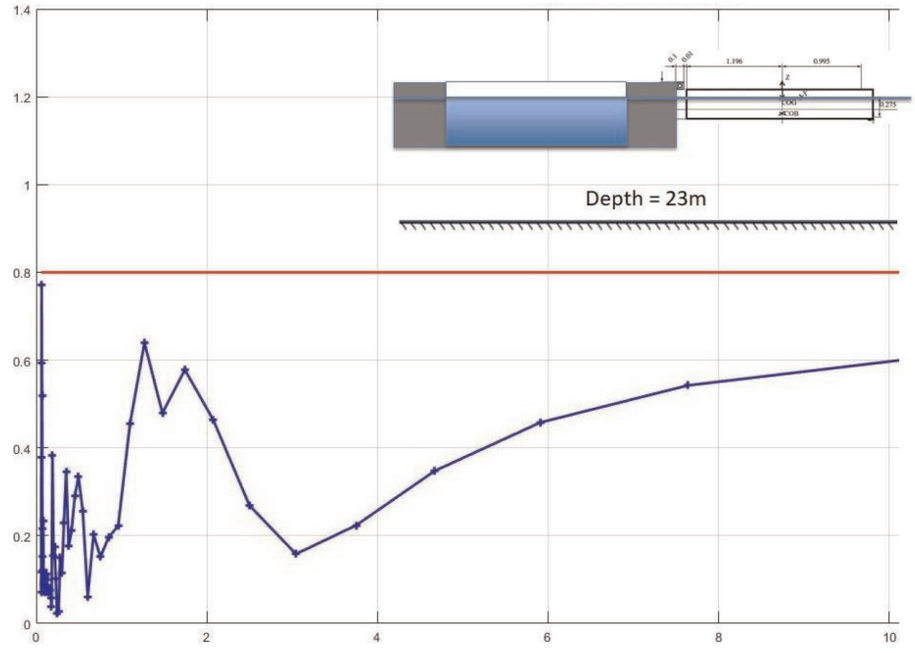

Figure 17.
Curves T/N and f_{grip} versus λ/B for 2 m Hs.

where:

$$
\begin{aligned}
&T_{\pm} \stackrel{\text{def}}{=} \tan(\omega t_{\pm}/2),\\
&A \stackrel{\text{def}}{=} Z_m \cos(-\omega t_T + \varphi_z),\\
&B \stackrel{\text{def}}{=} Z_m \sin(-\omega t_T + \varphi_z),\\
&C \stackrel{\text{def}}{=} X_m, \cos(-\omega t_N + \varphi_x) + Z_G \theta_m \cos(-\omega t_N + \varphi_\theta),\\
&D \stackrel{\text{def}}{=} X_m \sin(-\omega t_N + \varphi_x) + Z_G \theta_m \sin(-\omega t_N + \varphi_\theta).\\
&\mathcal{G} = -\min(L, |P_{max}|/[m\omega^2])\\
&P_{max} = \max\left\{(m + m_a)a\sqrt{g/h} \bullet \omega, \text{CTV maximum thruster force}\right\}
\end{aligned}
\tag{17}
$$

At the large wave periods we have the following behavior:

$$
\lim_{\omega \to 0} |f_{max}(T)| = \max\left\{\lim_{\omega \to 0} |f(T_-)|, \lim_{\omega \to 0} |f(T_+)|\right\} \tag{18}
$$

Where (see Eq. (11)):

$$T_{\pm} = \left(A\mathcal{G} \pm \sqrt{\{A^2 + B^2\}\mathcal{G}^2 - (AD - BC)^2} \right) / (AD - BC + B\mathcal{G}) \tag{19}$$

In the case of box barge of same displacement, length and draft, we have:

9.2 Surge amplitude at large wave periods

$$\frac{x_m}{a} = \frac{\sqrt{(\eta\omega^3 - \mathrm{Im}(\vartheta)\omega^2 + \mathrm{Re}(\kappa)\omega)^2 + (\zeta\omega^4 + \mathrm{Re}(\vartheta)\omega^2 + \mathrm{Im}(\kappa)\omega + \mathrm{Re}(\mu))^2}}{\sqrt{(\alpha\omega^6 + \gamma\omega^4 + \varepsilon\omega^2)^2 + (\beta\omega^5 + \delta\omega^3 + \epsilon\omega)^2}}$$

$$\mathrm{Re}(\kappa) \stackrel{\mathrm{def}}{=} \left[K_{55}b_3 + \left(\Lambda\omega H^3/3\right)k_3\right](\mathcal{F}_{xm}/a) + \left[\left(\Lambda\omega H^2/2\right)k_3\right](\mathcal{M}_{ym}/a)$$

$$\mathrm{Im}(\kappa) \stackrel{\mathrm{def}}{=} + \left[\left(\Lambda\omega H^2/2\right)P\right](\mathcal{F}_{zm}/a)$$

$$\mathrm{Re}(\mu) \stackrel{\mathrm{def}}{=} + \left(P^2 + K_{55}k_3\right)(\mathcal{F}_{xm}/a)$$

$$\varepsilon \stackrel{\mathrm{def}}{=} -(m + m_a)P^2 - b_3K_{55}(\Lambda H\omega) - k_3\left\{(m + m_a)K_{55} + \left[\left(\Lambda\omega H^2\right)^2/12\right]\right\}$$

$$\epsilon \stackrel{\mathrm{def}}{=} -(\Lambda H\omega)\left(P^2 + k_3K_{55}\right)$$

$$K_{55} \stackrel{\mathrm{def}}{=} -(\Delta g \bullet GC) + \Delta g\left[B^2/(12H)\right] + \left(KZ_A^{+2}\right)$$

$$k_3 \stackrel{\mathrm{def}}{=} (\Delta/H)g$$

$$\lim_{k \to 0}\frac{x_m}{a} = \lim_{\omega \to 0}\frac{\sqrt{(\mathrm{Re}(\kappa)\omega)^2 + (\mathrm{Im}(\kappa)\omega + \mathrm{Re}(\mu))^2}}{\sqrt{(\varepsilon\omega^2)^2 + (\epsilon\omega)^2}}$$

$$\lim_{\omega \to 0}\mathcal{F}_{xm}/a = O\left(\omega^3\right)$$

$$\lim_{\omega \to 0}\mathcal{M}_{ym}/a = \lim_{k \to 0}\left[\left\{(m + m_a)\frac{H}{2} - \Delta\frac{B^2}{12H}\right\}\sqrt{\frac{g}{h}}\omega + (m + m_a)\sqrt{\frac{g}{h}}\omega Z_a^+ + O\left(\omega^3\right)\right]$$

$$\lim_{\omega \to 0}\mathrm{Im}\mathcal{F}_{zm}/a = -(\Delta g/H)\{\sinh[k(z_0 + h)]/\sinh(kh)\} + O(\omega)$$

(20)

Note: since the vertical incident wave loads are only the ones passing below the floater keel then, if its draft is $|z_0|$, $z_m/a = z_m(z = z_0) = \sinh[k(z_0 + h)]/\sinh(kh)$ [12] (refer to equations written in **Figures 6, 9, 12**, and **15**).

Therefore:

$$\lim_{\omega \to 0}\mathrm{Re}(\kappa) = \lim_{\omega \to 0}O\left(\omega^3\right) + \left[\frac{\Lambda H^2}{2}k_3\right]\left\{(m + m_a)\left[Z_a^+ + \frac{H}{2}\right] - \Delta\frac{B^2}{12H}\right\}\sqrt{\frac{g}{h}}\omega^2$$

$$\lim_{\omega \to 0}\mathrm{Im}(\kappa) = \lim_{\omega \to 0}O\left(\omega^2\right)$$

$$\begin{aligned}
&\lim_{\omega \to 0} \mathrm{Re}\,(\mu) = \lim_{\omega \to 0} \left[\mathrm{O}\left(\omega^2\right) + \mathrm{K}_{55}\mathrm{k}_3\right]\mathrm{O}\left(\omega^3\right)\\
&\lim_{\omega \to 0} \varepsilon = \lim_{\omega \to 0} - \mathrm{k}_3(\mathrm{m} + \mathrm{m}_a)\mathrm{K}_{55} + \mathrm{O}(\omega)\\
&\lim_{\omega \to 0} \epsilon = \lim_{\omega \to 0} - (\Lambda \mathrm{H}\omega)\left(\mathrm{P}^2 + \mathrm{k}_3\mathrm{K}_{55}\right)\\
&\lim_{\mathrm{k} \to 0} \frac{\mathrm{x}_\mathrm{m}}{\mathrm{a}} = \lim_{\omega \to 0} \frac{\sqrt{[\mathrm{O}(\omega^3)]^2 + [\mathrm{O}(\omega^3) + (\mathrm{O}(\omega^2) + \mathrm{K}_{55}\mathrm{k}_3)\mathrm{O}(\omega^3)]^2}}{\sqrt{[-\mathrm{k}_3(\mathrm{m} + \mathrm{m}_a)\mathrm{K}_{55}\omega^2]^2 + [(\Lambda \mathrm{H})(\mathrm{O}(\omega^2) + \mathrm{k}_3\mathrm{K}_{55})\omega^2]^2}}\\
&\lim_{k \to 0} x_m/a = O(\omega)
\end{aligned} \tag{21}$$

9.3 Surge phase angle at large wave periods

$$\begin{aligned}
\cos\varphi_\mathrm{x} = &\left\{+[\eta\omega^3 - \mathrm{Im}(\vartheta)\omega^2 + \mathrm{Re}\,(\kappa)\omega]\left(\alpha\omega^6 + \gamma\omega^4 + \varepsilon\omega^2\right)\right.\\
&\left.+[\zeta\omega^4 + Re\,(\vartheta)\omega^2 + Im(\kappa)\omega + Re\,(\mu)](\beta\omega^5 + \delta\omega^3 + \epsilon\omega)\right\}\\
&/\sqrt{(\alpha\omega^6 + \gamma\omega^4 + \varepsilon\omega^2\imath)^2 + (\beta\omega^5 + \delta\omega^3 + \epsilon\omega)^2}\\
&/\sqrt{[\eta\omega^3 - \mathrm{Im}(\vartheta)\omega^2 + \mathrm{Re}\,(\kappa)\omega]^2 + [\zeta\omega^4 + \mathrm{Re}\,(\vartheta)\omega^2 + \mathrm{Im}(\kappa)\omega + \mathrm{Re}\,(\mu)]^2}\\
\sin\varphi_\mathrm{x} = &\left\{+[\eta\omega^3 - \mathrm{Im}(\vartheta)\omega^2 + \mathrm{Re}\,(\kappa)\omega](\beta\omega^5 + \delta\omega^3 + \epsilon\omega)\right.\\
&\left.-[\zeta\omega^4 + \mathrm{Re}\,(\vartheta)\omega^2 + \mathrm{Im}(\kappa)\omega + \mathrm{Re}\,(\mu)]\left(\alpha\omega^6 + \gamma\omega^4 + \varepsilon\omega^2 + \imath\right)\right\}\\
&/\sqrt{(\alpha\omega^6 + \gamma\omega^4 + \varepsilon\omega^2\imath)^2 + (\beta\omega^5 + \delta\omega^3 + \epsilon\omega)^2}\\
&/\sqrt{[\eta\omega^3 - \mathrm{Im}(\vartheta)\omega^2 + \mathrm{Re}\,(\kappa)\omega]^2 + [\zeta\omega^4 + \mathrm{Re}\,(\vartheta)\omega^2 + \mathrm{Im}(\kappa)\omega + \mathrm{Re}\,(\mu)]^2}\\
&c_\Lambda \stackrel{\mathrm{def}}{=} \Lambda H/(m + m_a)\\
&\lim_{T \to +\infty} \cos\varphi_x = -c_\Lambda/\sqrt{1 + {c_\Lambda}^2}\\
&\lim_{T \to +\infty} \sin\varphi_x = 1/\sqrt{1 + {c_\Lambda}^2}
\end{aligned} \tag{22}$$

9.4 Heave amplitude at large wave periods

$$\begin{aligned}
&\frac{\mathrm{z}_\mathrm{m}}{\mathrm{a}} = \frac{\sqrt{[-\mathrm{Im}(\Gamma)\omega^4 - \mathrm{Im}(\Pi)\omega^2 + \mathrm{Re}\,(\Sigma)\omega]^2 + [\mathrm{Im}(\Xi)\omega^3 + \mathrm{Re}\,(\Pi)\omega^2 + \mathrm{Im}(\Sigma)\omega]^2}}{\sqrt{[\alpha\omega^6 + \gamma\omega^4 + \varepsilon\omega^2]^2 + [\beta\omega^5 + \delta\omega^3 + \epsilon\omega]^2}}\\
&\mathrm{Re}\,(\Pi) \stackrel{\mathrm{def}}{=} [\mathrm{I}_{\mathrm{GA}15}\mathrm{P}](\mathcal{F}_{\mathrm{xm}}/\mathrm{a}) - [(\mathrm{m} + \mathrm{m}_\mathrm{a})\mathrm{P}]\left(\mathcal{M}_{\mathrm{ym}}/\mathrm{a}\right)\\
&\mathrm{Im}(\Pi) \stackrel{\mathrm{def}}{=} \left\{(\mathrm{m} + \mathrm{m}_\mathrm{a})\mathrm{K}_{55} + \mathrm{B}_{11}\mathrm{B}_{55} - \mathrm{B}_{15}^2\right\}\mathrm{Im}(\mathcal{F}_{\mathrm{zm}}/\mathrm{a})\\
&\mathrm{Re}\,(\Sigma) \stackrel{\mathrm{def}}{=} -[\mathrm{B}_{15}\mathrm{P}](\mathcal{F}_{\mathrm{xm}}/\mathrm{a}) + [\mathrm{B}_{11}\mathrm{P}]\left(\mathcal{M}_{\mathrm{ym}}/\mathrm{a}\right)\\
&\mathrm{Im}(\Sigma) \stackrel{\mathrm{def}}{=} -[\mathrm{K}\mathrm{B}_{55} + \mathrm{K}_{55}\mathrm{B}_{11}]\mathrm{Im}(\mathcal{F}_{\mathrm{zm}}/\mathrm{a})
\end{aligned}$$

$$
\begin{aligned}
&I_{GA15} \stackrel{\text{def}}{=} mz_G - (m_{a1}H/2)\\
&B_{11} \stackrel{\text{def}}{=} \lambda H\\
&B_{15} \stackrel{\text{def}}{=} -\left(\lambda H^2/2\right)\\
&B_{55} \stackrel{\text{def}}{=} \Lambda\omega H^3/3\\
&\frac{lim}{k \to 0} z_m/a = \sinh\left[k(z_0+h)\right]/\sinh(kh)
\end{aligned}
\tag{23}
$$

9.5 Heave phase angle at large wave periods

$$
\begin{aligned}
\cos\varphi_z = &\left\{-[-\mathrm{Im}(\Gamma)\omega^4 - \mathrm{Im}(\Pi)\omega^2 + \mathrm{Re}(\Sigma)\omega]\left(\alpha\omega^6 + \gamma\omega^4 + \varepsilon\omega^2\right)\right.\\
&\left.-[\mathrm{Im}(\Xi)\omega^3 + \mathrm{Re}(\Pi)\omega^2 + \mathrm{Im}(\Sigma)\omega](\beta\omega^5 + \delta\omega^3 + \epsilon\omega)\right\}\\
&/\sqrt{[-\mathrm{Im}(\Gamma)\omega^4 - \mathrm{Im}(\Pi)\omega^2 + \mathrm{Re}(\Sigma)\omega]^2 + [\mathrm{Im}(\Xi)\omega^3 + \mathrm{Re}(\Pi)\omega^2 + \mathrm{Im}(\Sigma)\omega]^2}\\
&/\sqrt{[\alpha\omega^6 + \gamma\omega^4 + \varepsilon\omega^2]^2 + [\beta\omega^5 + \delta\omega^3 + \epsilon\omega]^2}\\
\sin\varphi_z = &\left\{+[-\mathrm{Im}(\Gamma)\omega^4 - \mathrm{Im}(\Pi)\omega^2 + \mathrm{Re}(\Sigma)\omega](\beta\omega^5 + \delta\omega^3 + \epsilon\omega)\right.\\
&\left.+[\mathrm{Im}(\Xi)\omega^3 + \mathrm{Re}(\Pi)\omega^2 + \mathrm{Im}(\Sigma)\omega]\left(\alpha\omega^6 + \gamma\omega^4 + \varepsilon\omega^2\right)\right\}\\
&/\sqrt{[-\mathrm{Im}(\Gamma)\omega^4 - \mathrm{Im}(\Pi)\omega^2 + \mathrm{Re}(\Sigma)\omega]^2 + [\mathrm{Im}(\Xi)\omega^3 + \mathrm{Re}(\Pi)\omega^2 + \mathrm{Im}(\Sigma)\omega]^2}\\
&/\sqrt{[\alpha\omega^6 + \gamma\omega^4 + \varepsilon\omega^2]^2 + [\beta\omega^5 + \delta\omega^3 + \epsilon\omega]^2}
\end{aligned}
\tag{24}
$$

$$
\lim_{T \to +\infty} \varphi_z = 0^\circ
$$

9.6 Pitch amplitude at large wave periods

$$
\begin{aligned}
&\frac{\theta_m}{a} = \frac{\sqrt{\{\mathrm{Re}(\mathbb{D})\omega^3 + \mathrm{Re}(\mathbb{E})\omega^2 + \mathrm{Re}(\mathbb{F})\omega\}^2 + \{\mathrm{Im}(\mathbb{C})\omega^4 + \mathrm{Im}(\mathbb{E})\omega^2 + \mathrm{Im}(\mathbb{F})\omega\}^2}}{\sqrt{\{\alpha\omega^6 + \gamma\omega^4 + \varepsilon\omega^2\}^2 + \{\beta\omega^5 + \delta\omega^3 + \epsilon\omega\}^2}}\\
&\mathrm{Re}(\mathbb{E}) \stackrel{\text{def}}{=} -\{-[(m+m_a)P]\mathrm{Im}(\mathcal{F}_{zm}/a)\} = -(m+m_a)P\Delta g/H\\
&\mathrm{Im}(\mathbb{E}) \stackrel{\text{def}}{=} \left[I_{GA15} - (m+m_a)Z_a^+\right]k_3(P/a)\\
&\mathrm{Re}(\mathbb{F}) \stackrel{\text{def}}{=} -\left\{[k_3B_{15}](\mathcal{F}_{xm}/a) - [k_3B_{11}]\left(\mathcal{M}_{ym}/a\right)\right\}\\
&\mathrm{Im}(\mathbb{F}) \stackrel{\text{def}}{=} -\{-[B_{11}P]\mathrm{Im}(\mathcal{F}_{zm}/a)\}\\
&\lim_{k \to 0}\frac{\theta_m}{a} = \lim_{\omega \to 0}\frac{(m+m_a)\sqrt{g/h}\omega}{K_{55}}\sqrt{\left\{\left[\frac{H}{2} + Z_a^+\right] - [\Delta/(m+m_a)]\frac{B^2}{12H}\right\}^2 + a^2}\\
&\frac{lim}{k \to 0}\theta_m/a = 0
\end{aligned}
\tag{25}
$$

9.7 Pitch phase angle at large wave periods

$$\cos\varphi_\theta = \{+[\mathrm{Re}(\mathbb{D})\omega^3 + \mathrm{Re}(\mathbb{E})\omega^2 + \mathrm{Re}(\mathbb{F})\omega](\alpha\omega^6 + \gamma\omega^4 + \varepsilon\omega^2)$$
$$+[\mathrm{Im}(\mathbb{C})\omega^4 + \mathrm{Im}(\mathbb{D})\omega^3 + \mathrm{Im}(\mathbb{E})\omega^2 + \mathrm{Im}(\mathbb{F})\omega](\beta\omega^5 + \delta\omega^3 + \epsilon\omega)\}$$
$$/\sqrt{\{\mathrm{Re}(\mathbb{D})\omega^3 + \mathrm{Re}(\mathbb{E})\omega^2 + \mathrm{Re}(\mathbb{F})\omega\}^2 + \{\mathrm{Im}(\mathbb{C})\omega^4 + \mathrm{Im}(\mathbb{D})\omega^3 + \mathrm{Im}(\mathbb{E})\omega^2 + \mathrm{Im}(\mathbb{F})\omega\}^2}$$
$$/\sqrt{\{\alpha\omega^6 + \gamma\omega^4 + \varepsilon\omega^2\}^2 + \{\beta\omega^5 + \delta\omega^3 + \epsilon\omega\}^2}$$

$$\sin\varphi_\theta = \{+[\mathrm{Re}(\mathbb{D})\omega^3 + \mathrm{Re}(\mathbb{E})\omega^2 + \mathrm{Re}(\mathbb{F})\omega](\beta\omega^5 + \delta\omega^3 + \epsilon\omega)$$
$$-[\mathrm{Im}(\mathbb{C})\omega^4 + \mathrm{Im}(\mathbb{D})\omega^3 + \mathrm{Im}(\mathbb{E})\omega^2 + \mathrm{Im}(\mathbb{F})\omega](\alpha\omega^6 + \gamma\omega^4 + \varepsilon\omega^2)\}$$
$$/\sqrt{\{\mathrm{Re}(\mathbb{D})\omega^3 + \mathrm{Re}(\mathbb{E})\omega^2 + \mathrm{Re}(\mathbb{F})\omega\}^2 + \{\mathrm{Im}(\mathbb{C})\omega^4 + \mathrm{Im}(\mathbb{D})\omega^3 + \mathrm{Im}(\mathbb{E})\omega^2 + \mathrm{Im}(\mathbb{F})\omega\}^2}$$
$$/\sqrt{\{\alpha\omega^6 + \gamma\omega^4 + \varepsilon\omega^2\}^2 + \{\beta\omega^5 + \delta\omega^3 + \epsilon\omega\}^2}$$

$$\begin{cases} \lim\limits_{T\to+\infty}\cos\varphi_\theta = \dfrac{1}{\sqrt{1+\left\{-\left(Z_a^+/a\right)-\left[(1/2)-\left\{B^2/\left[12H^2(1+C_{m1})\right]\right\}\right](H/a)\right\}^2}} \\ \lim\limits_{T\to+\infty}\sin\varphi_\theta = \dfrac{-\left(Z_a^+/a\right)-\left[(1/2)-\left\{B^2/\left[12H^2(1+C_{m1})\right]\right\}\right]}{\sqrt{1+\left\{-\left(Z_a^+/a\right)-\left[(1/2)-\left\{B^2/\left[12H^2(1+C_{m1})\right]\right\}\right](H/a)\right\}^2}} \end{cases} \quad (26)$$

$$\varphi'''_{x1} \stackrel{\text{def}}{=} \left(Z_a^+/a\right) + \left\{\left[(1/2)-\left\{B^2/\left[12H^2(1+C_{m1})\right]\right\}\right](H/a)\right\}$$

$$\lim_{\omega\to0}\cos\varphi_\theta = 1/\sqrt{1+\varphi'''^2_{x1}}$$

$$\lim_{\omega\to0}\sin\varphi_\theta = -\varphi'''_{x1}/\sqrt{1+\varphi'''^2_{x1}}$$

9.8 Friction coefficient at large wave periods

Therefore:

$$\lim_{\omega\to0}A = \lim_{\omega\to0}a\{\sinh[k(z_0+h)]/\sinh(kh)\}\bullet\cos 360^\circ = a(z_0+h)/h,$$
$$\lim_{\omega\to0}B = \lim_{\omega\to0}a\{\sinh[k(z_0+h)]/\sinh(kh)\}\bullet(-\omega t_T) = O(\omega)$$
$$\lim_{\omega\to0}C = O(\omega)\left(-c_\Lambda/\sqrt{1+c_\Lambda{}^2}\right) + Z_G O(\omega)\left(1/\sqrt{1+\varphi'''^2_{x1}}\right) = O(\omega),$$
$$\lim_{\omega\to0}D = O(\omega)\left(1/\sqrt{1+c_\Lambda{}^2}\right) + Z_G O(\omega)\left(-\varphi'''_{x1}/\sqrt{1+\varphi'''^2_{x1}}\right) = O(\omega)$$
$$\lim_{\omega\to0}\mathcal{G} = (-L) \quad (27)$$

$$\lim_{\omega\to0}T_\pm = \lim_{\omega\to0}\frac{A(-L)\mp\sqrt{\left\{A^2+O(\omega)^2\right\}L^2-[AO(\omega)-O(\omega)O(\omega)]^2}}{[AO(\omega)-O(\omega)O(\omega)+O(\omega)(-L)+O(\omega)(-L)]}$$
$$\lim_{\omega\to0}T_\pm = \lim_{\omega\to0}\left[-AL\mp\left\{AL+O(\omega^2)\right\}\right]/O(\omega)$$
$$\lim_{\omega\to0}T_- = \underset{\omega\to0}{\mathrm{LIM}}[-[a(z_0+h)/h]L-[a(z_0+h)/h]L+O(\omega)]/O(\omega) = \infty$$

Case	Floater geometry	Depth	Maximum Hs for berthing (Hs = 2a)[1]
1	5 m diameter monopile	23 m	1.5 m (no masking)
2	13 m diameter cylindrical floater	70 m	2.0 m
3	41 m diameter cylindrical floater	23 m	2.3 m
4	36 m side square floater	23 m	2.3 m
5	36 m side square hollow floater (FLOATGEN)	23 m	2.3 m

[1]*The CAT CTV fender length is L = 1 m [1].*

Table 2.
CAT CTV analytical berthing limits for monopile various floater designs.

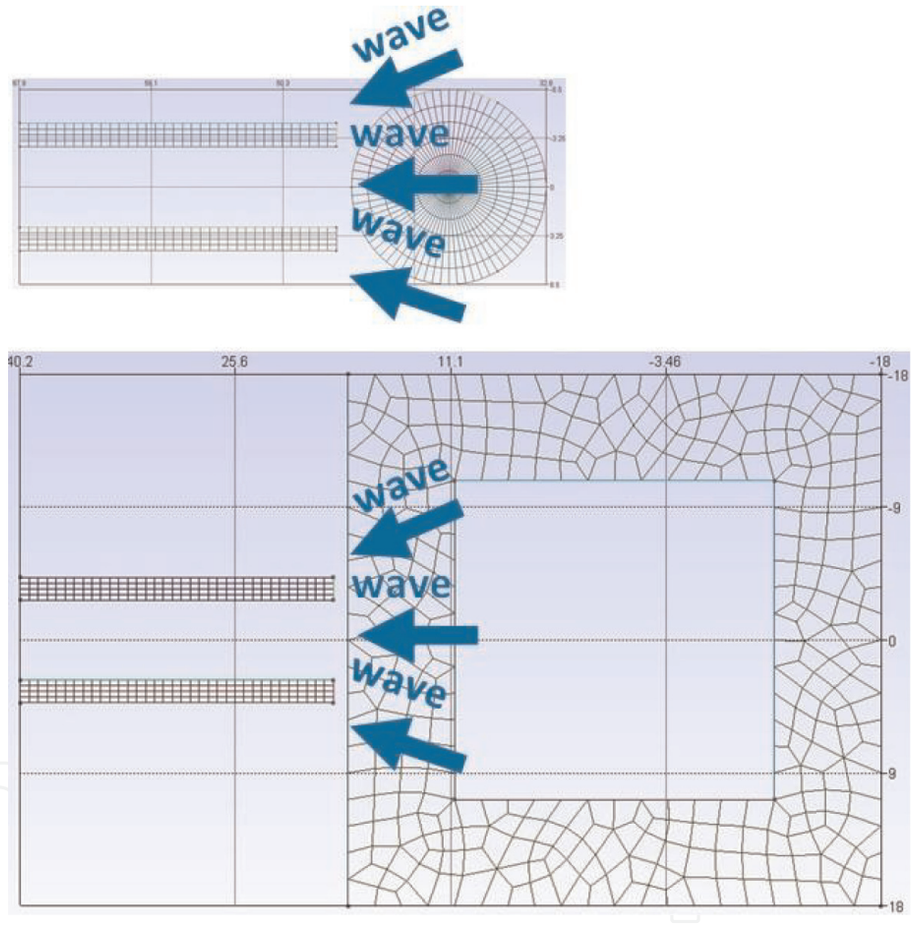

Figure 18.
Floater wave masking performances (cylinder versus FLOATGEN).

$$\lim_{k\to 0}|f(T_-)| = \left|\frac{-A-2\bullet 0+\{A\bullet 0^2\}}{-(0-[-L])-2\bullet 0+\left[(0+[-L])\bullet 0^2\right]}\right| = \frac{[a(z_0+h)/h]}{L}$$

$$\lim_{\omega\to 0} T_+ = \underset{\omega\to 0}{\mathrm{LIM}}[-AL+AL+O(\omega^2)]/O(\omega) = O(\omega) = 0 \tag{28}$$

$$\lim_{k\to 0}|f(T_+)| = \left|\frac{-A\bullet 0^2-2\bullet 0\bullet 0+A}{-(0-[-L])\bullet 0^2-2\bullet \mathrm{D}\bullet 0+(0+[-L])}\right| = \frac{[a(z_0+h)/h]}{L}$$

Eventually, we get the following formula for berthing to possible [1]:

$$\lim_{k\to 0} |f(T_{\pm})| = [a(z_0 + h)/h]/L < f_{grip} \tag{29}$$

$$\text{if } f_{grip} = 0,8 \ (rubber - very\ wet\ soil) \ (\text{refer to Eq.}(9))$$

Table 2 sums up the analytical Hs found for berthing to occur whatever the wavelength, by using Eq. (29).

As can be seen results from **Tables 1** and **2** meet with less than 12% discrepancy. The reason why is that the analytical calculation does not account for the diffraction forces.

Eventually, some practical considerations must be accounted for (see **Figure 18**):

The more the wave direction varies, the more a large floater width becomes necessary to allow berthing by masking the waves.

10. Conclusions and recommendations

The present study results find that berthing a CTV against an offshore wind turbine is not yet optimized, at least from a marine maintenance point of view: most designs do not provide sheltered waters.

Some proposals focus on improving the CTV:

- ESNA promote the use of Surface Effect Ships (SES), to minimize their heave. However, the lack of commercial success of the solution seems related to the high fuel consumption of such boats [7].

Other proposals focus rather on the floater side:

- IDEOL have designed a pontoon-like floater which provides sheltered waters. At best that solution will prove successful for floating wind farms. Obviously, that is not a solution for fixed wind farms [11].
- FLOATING POWER POINT propose a floating wind turbine combined with a wave energy convertor (WEC), to provide an artificial harbor downstream, thanks to the wave energy extracted by the WEC [13].

Another possible axis of development would be to design an additional wall to existing boat landings, providing a sheltered water.

Eventually, since the present study only applies to a unidirectional wave, the next studies will focus on multidirectional waves, in order represent a more realistic sea state.

Acknowledgements

The author gratefully acknowledges the support from ENSM and its director of research and industrial relations, Mr. Dominique FOLLUT, for throughout the present research work.

Acronyms and abbreviations

Abbreviation and definition

Cat	Catamaran
CTV	crew transfer vessel
DP	dynamic positioning
H_s	significant wave height
HSVA	Hamburgische Schiffbau-Versuchsanstalt GmbH (Hamburg Ship Model Tank Test Facilities)
O&M	operation & maintenance
RAO's	response amplitude operators
3D	three dimensional
2D	two dimensional
WT	wind turbine

Terminology and designation

O, x, y, z	absolute reference frame
M	operating point fixed to the CTV
ρ	water specific gravity
h	water depth
B	ship length
H	ship draft
m (or Δ)	ship mass (or displacement)
G	ship centre of gravity
I_G	ship inertia at G
C	ship centre of buoyancy
I	matrix of ship own inertia
I_a	matrix of ship added inertia
K	matrix of stiffnesses
B	matrix of dampings
F_{excit}	vector of wave loads
λ	wavelength
A-	berthing point
O, X, Y, Z	reference frame attached to the ship
F	centre of floatation
g	gravitational acceleration
x_G, z_G	coordinates of ship gravity centre
x_C, z_C	coordinates of ship buoyancy centre
b_3	ship heave damping factor
k_3	ship vertical hydrostatic stiffness
C_d	shipdrag coefficient
C_{m1}	added mass coefficient in x direction
m_a	added mass in x direction
X	vector of ship motions
τ_x	ship surge
τ_z	ship heave
θ	ship pitch angle
T	regular wave period

k	wave number
a	wave amplitude (half crest to through)
x (or b_c)	flat rate heave damping coefficient (%-age of critical damping)
x_{max} or τ_{xm}	max. surge estimate (for quadratic damping force)
ω	wave pulsation
θ_{max}	adimensional max. pitch estimate (for quadratic damping force)
Λ	$4\rho C C_d(x_{max} + H\theta_{max})/(3\pi)$
c_Λ	$\Lambda H/(m + m_a)$
$\mathcal{G}$	CTV surge over which the CTV captain has the time to adjust the propeller thrust P, in order for the fender never to lose contact with the boat landing
x_m	max. CTV surge
z_m	max. CTV heave
θ_m	max. CTV pitch
φ_x	max. CTV surge
φ_z	max. CTV heave
φ_θ	max. CTV pitch
L	fender length
Z_a^+	CTV propeller elevation
Z_0	floater keel elevation

Author details

Laurent Barthélemy
Ecole Nationale Supérieure Maritime, Nantes, France

*Address all correspondence to: laurent.barthelemy@supmaritime.fr

References

[1] Barthélemy. Berthing criteria for wind turbine crew transfer vessel with low or high friction fender. In: Proceedings of the 5th World Conference on Smart Trends in Systems, Security and Sustainability (World S4 '21); 29–30 July 2021. London, UK: IEEE/ Springer; forthcoming

[2] König M, Ferreira González D, Abdel-Maksoud M, Düster A. Numerical investigation of the landing manoeuvre of a crew transfer vessel to an offshore wind turbine. Ships and Offshore Structures. 2017;**12**(Suppl. 1):S115-S133. DOI: 10.1080/17445302.2016.1265883

[3] Carbon Thrust. Crew Transfer Vessel (CTV) Performance Plot (P-Plot) Development Notice to the Offshore Wind Energy Sector. 2017. Available from: https://www.carbontrust.com/media/674745/carbon-trust-p-plot-development-researchsummary-june-2017.pdf [Accessed: 13 May 2019]

[4] Available from: http://gmsh.info/ [Accessed: 01 August 2019]

[5] Babarit A, Delhommeau G. Theoretical and numerical aspects of the open source BEM solver NEMOH. In: Ecole Centrale Nantes, 11th European Wave and Tidal Energy Conference (EWTEC 2015); Nantes, France. 2015. Available from: https://lheea.ec-nantes.fr/logiciels-et-brevets/nemoh-presentation-192863.kjsp [Accessed: 12 July 2019]

[6] Muller J. Formulaire technique de Mécanique Générale 16è édition—Théorie et dimensionnement. DUNOD. 2015. Available from: http://maron.perso.univ-pau.fr/meca_old/ch3coef.htm [Accessed: 01 May 2019]

[7] Skomedal NG, Espeland TH. Cost-effective surface effect ships for offshore wind. Esna AS, Kristiansand S, Norway, FAST 2017 Conference; Nantes, France. 2017

[8] Available from: https://info-efgl.fr/le-projet/le-flotteur-ppi-eiffage/ [Accessed: 29 October 2021]

[9] Available from: https://www.energiesdelamer.eu/bin/statsnews.php?lst=2&nid=395&img=publications/4085-bouygues-travaux-publics-presente-le-flotteur-floatgen-au-concours-tekla [Accessed: 03 June 2018]

[10] Weller S. Fibre rope selection for offshore renewable energy: Current status and future needs. In: Tension Technology International Ltd EUROMECH 607, Brest; 29th August 2019. Available from: https://wwz.ifremer.fr/rd_technologiques/content/download/136107/file/Session%204%20Weller.pdf [Accessed: 02 January 2020]

[11] Ideol TC. IDEOL'S French and Japanese demonstrators: A necessary stepping stone on the way to commercial-scale projects. In: Conference FOWT 2019; Montpellier, France. 2019

[12] Le Boulluec M. «CRE-1-Houle-MLB». Cours 2015-2016 de Mastère Spécialisé Energies Marines Renouvelables. Ecole Nationale Superieure Des Techniques Avancees; Brest, France. 2015

[13] Available from: https://www.floatingpowerplant.com/ [Accessed: 28 October 2021]